JOURNAL OF MATERIALS SCIENCE 12 (1977) 583–594

# The microstructure of fluidizable cracking catalysts

JONATHAN L. BASS, RONALD E. RITTER
*Davison Chemical Division, W. R. Grace & Co, Washington Research Center, Columbia, Maryland, USA*

The characteristic morphologies of components used to prepared fluidizable cracking catalysts have been identified in formed microspheres by a scanning electron microscope–energy dispersive X-ray analyser system. Differences in preparation methods and materials are observed in the catalyst microstructure. Cracking unit processes and laboratory simulation experiments result in changes in catalyst morphology. The relationships between cracking catalyst microstructure and performance are discussed in this paper.

## 1. Introduction

Cracking catalysts used by the petroleum industry to convert heavy feedstocks to lighter products such as gasoline are usually characterized physically by particle size, pore volume, surface area, bulk density, and attrition resistance. These parameters are determined by measurements averaged over a large number of particles. The microscopic examination of individual cracking catalyst particles provides an additional powerful technique for monitoring their preparation and understanding how they perform in fluidized cracking units.

Many grades of cracking catalyst, differing from one another in chemical composition and/or physical properties, are available to meet the varying operating requirements of refinery fluidized cracking units throughout the world. The most common fluidizable cracking catalysts are aluminosilicate spheroids ranging from 30 to 150 $\mu$m diameter. The resolution and depth of field of an optical microscope is inadequate for studying the surface texture of the microspheroid. Although the materials comprising a cracking catalyst particle such as gel, clay or zeolite have been studied separately by transmission electron microscopy (TEM) [1-3], the examination of a whole particle by TEM requires difficult sectioning or replication techniques. Scanning electron microscopy (SEM) can be used to examine the catalyst, without extensive sample preparation, with spatial resolution of about 100 Å. An energy dispersive X-ray analyser (EDXRA), which collects X-rays emitted when the electron beam of the SEM interacts with the sample, can be used for a qualitative determination of the elemental composition of interesting morphological features in the microscopic field of view [4].

Prior applications of scanning electron microscopy to studying catalysts have mainly concerned systems other than cracking catalysts. The texture of Raney nickel surfaces was investigated by Robertson *et al.* [5]. The effects of moisture on boron phosphate were studied by Moffat and Brauneisen [6]. The morphology of commonly used catalyst supports such as alumina and silica has been examined by Faulker *et al.* [7], Waldie [8] and Bossi *et al.* [9]. The relationship between morphology and changes in catalytic activity for sulphur dioxide removal was studied by Reimschussel and Fredericks [10]. The effect of thermal shock on cracking catalysts was illustrated by Edgar [11]. In this paper we discuss several areas where the microstructural examination of cracking catalysts by SEM has led to greater understanding of their physical properties.

## 2. Experimental

Cracking catalyst microstructure was examined using a Cambridge Stereoscan mark II-A scanning electron microscope in combination with an EDAX, International energy dispersive X-ray

analyser system. The spatial resolution of the SEM is about 100 Å and the energy resolution of the X-ray detector is 175 keV at 6.4 keV, well suited for resolving the silicon and aluminium *K* lines, the two most important in the spectra of cracking catalysts.

The catalyst particles are normally coated with a 60% Au–40% Pd/alloy to minimize surface charge accumulation. This film is about 100 to 150 Å thick. Particles removed from a cracking unit which are covered with a coke layer may not accumulate surface charge, but the coke layer may obscure surface detail. Also, poor secondary electron emission from the coke may reduce resolution. The X-ray lines of gold and palladium do not interfere with those of the important elements present in cracking catalysts.

The cracking catalysts described in this work were prepared by gelling a slurry of sodium silicate and clay, and then adding sodium aluminate to obtain an aluminosilicate gel. Crystalline aluminosilicate zeolites may be added to obtain a more hydrothermally stable and active catalyst. The composite is then formed into fluidizable particles (20 to 150 $\mu$m) by spray drying and washed to remove soluble impurities [12–14]. Before SEM examination, the catalysts are either calcined in air at 540° C for 4 h to reduce volatile content to less than 1 wt% ("fresh" catalyst), or steam deactivated to approximate the activity and pore structure of used catalyst circulated in refinery cracking units. Comparisons between used and laboratory-steamed catalysts show that deactivation at either 740° C in a 100% steam atmosphere for 8 h or 825° C in a 20% steam-80% air atmosphere for 12 h, depending on catalyst grade, provides the best simulation.

Several cracking catalyst samples were subjected to an attrition test using the standard Roller particle size analyser manufactured by American Instrument Co, Inc. This test utilized air impingement at a nozzle exit velocity of about 460 ft $sec^{-1}$ * to simulate the attrition that occurs when catalyst particles are circulated in a refinery cracking unit. Particles less than 20 $\mu$m in size are removed by the air stream and samples of the remaining particles were examined by SEM to visually determine the mechanism of attrition. Micromesh analyses involving separation of the samples into several particles size ranges were accomplished by vibrating the catalyst through a series of standard sized screens for 30 min and weighing the portion collected on each screen.

## 3. Results and discussion

### 3.1. Microstructure of cracking catalysts

The activity of a cracking catalyst is measured by its ability to convert a high molecular weight petroleum fraction to desired lower molecular weight products such as gasoline (petrol) or fuel oil. Our laboratory evaluations of catalyst preparations determine the volume percentage con-

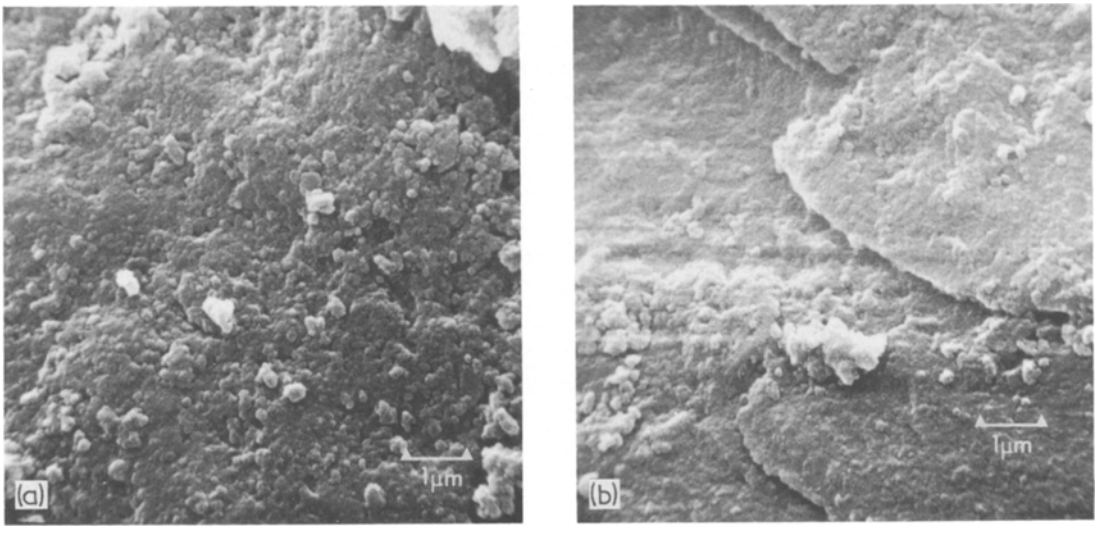


*Figure 1* (a) Surface of amorphous cracking catalyst, × 8500. (b) Interior of amorphous cracking catalyst, × 8500.

*1 ft $sec^{-1}$ = 3.0480 × $10^{-1}$ m $sec^{-1}$.

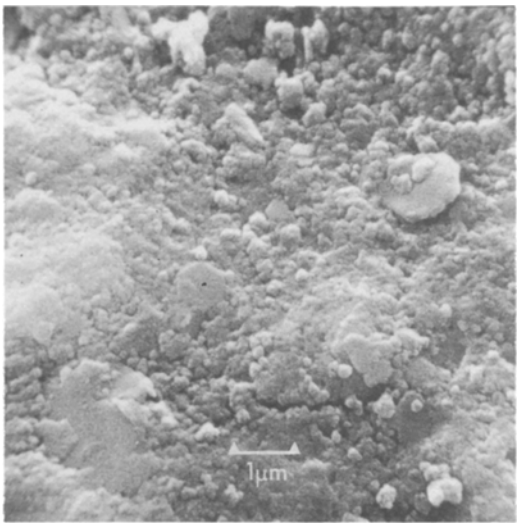


*Figure 2* Surface of zeolite cracking catalyst, × 8500.

version of a feedstock to gasoline and lighter products, using steam deactivated samples.

The first synthetic cracking catalysts were amorphous aluminosilicate gels whose alumina content ranged up to 25% $Al_2O_3$ by weight. Fig. 1 illustrates the granular surface and interior morphology of amorphous catalysts. The activity of such a catalyst after an 825° C, 20% steam deactivation, is approximately 40 vol % conversion. More recently developed cracking catalysts [12, 13] are a combination of gel, clay and zeolite components. These catalysts are more active for conversion to gasoline and lighter products, with activities ranging from 70 to 80 vol % conversion, after deactivation under conditions which simulate refinery operations. Fig. 2 shows the morphology of the surface of this type of catalyst. It is apparent that the spray drying step used during catalyst preparation obscures the characteristic morphologies of the three components. However, when we lightly grind a catalyst containing zeolite and examine the interior of fractured particles, the presence of granular gel, octahedral zeolites and platelet kaolin particles can clearly be observed (see Fig. 3, 3(a) and (d)).

Table I gives the chemical analysis of a typical cracking catalyst. The major elements are silicon and aluminium. The relative amounts of these two

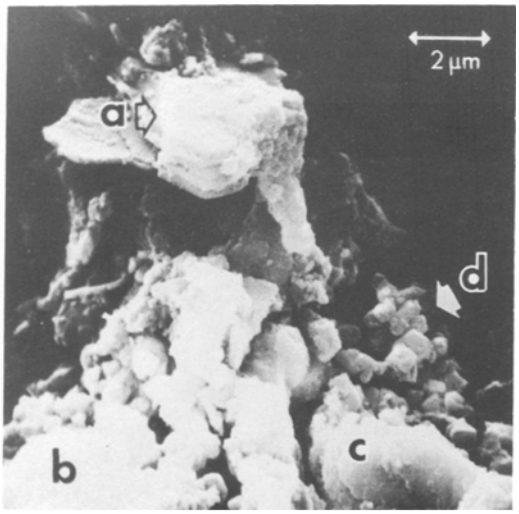


*Figure 3* Interior of zeolite cracking catalyst, × 4250: a and c, kaolin platelets, b, gel, and d, zeolites. (a) is area a, × 8500. (d) is area d, × 17 000.

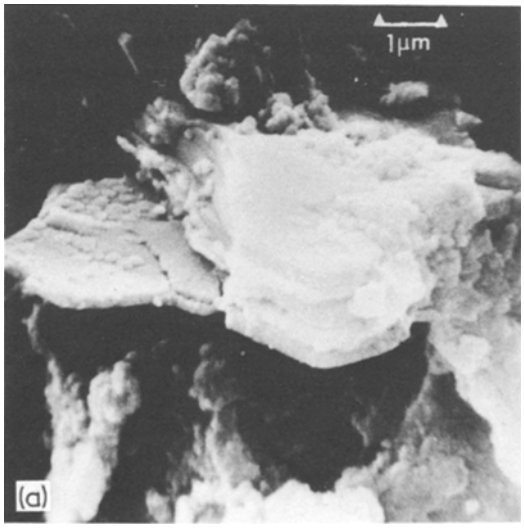


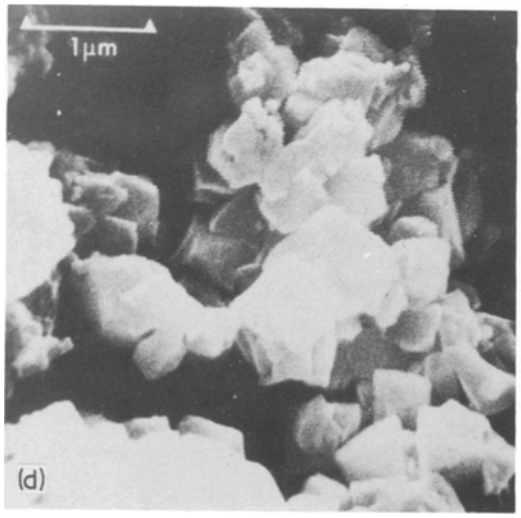

TABLE I Chemical analysis of a typical cracking catalyst

| | Wt % |
|---|---|
| $Al_2O_3$ | 28.0 |
| $RE_2O_3$ * | 4.49 |
| $Na_2O$ | 0.53 |
| $SO_4^{2-}$ | 0.49 |
| $TiO_2$ | 0.39 |
| Fe | 0.085 |
| $SiO_2$ † | 66.0 |

*Rare earth oxides are a mixture of mainly cerium, lanthanum and neodymium oxides where the relative proportion of each element varies with the source of rare earth salts used in catalyst preparation.

†Silica content is not analysed directly but is considered to account for the remainder of the chemical composition after the percentages of the other elements are determined.

elements vary for the different components within a microsphere and this variation may be used to aid in identifying a particle. However, the X-ray spectrum of a particular component in a microsphere may differ from the spectrum obtained when the component is examined separately because of secondary fluorescence and absorption by the other components. Fig. 4 shows that the clay particles of Fig. 1 contain more aluminium than the zeolites. Kaolin is about 45% alumina by weight, while zeolites used in cracking catalysts are about 25 to 40% alumina by weight. Rare earth elements, mainly lanthanum and cerium, are concentrated in zeolites to enhance sieve stability and cracking activity. The X-ray spectra of these elements appear as weak peaks above the background in the 4.5 to 5.5 keV region. The characteristic X-rays of the rare earths detected by our system are $L$ lines, with a lower fluorescent yield compared to the $K$ lines [15] observed for the other elements usually found in cracking catalysts. The detection limit for rare earths is about 1%, compared to 0.1 to 0.5% for other minor elements such as titanium, iron, nickel and vanadium.

Elements commonly found in minor amounts in cracking catalysts are titanium, sodium, iron, chromium, sulphur, nickel and vanadium. Titania in clay-based catalysts normally occurs in the range from 0.5 to 2 wt % according to bulk chemical analysis. However, single element X-ray mapping of titanium distribution shows localized concentrations of titania (Fig. 5a), in the catalyst particles of Fig. 5b. The substantially higher local concentration of titania is confirmed by comparing the titanium region (Fig. 5c) of the EDXRA spectrum for one of these areas (light lines) with the spectrum averaged over hundreds of microspheres (bright lines), which is similar to a bulk analysis. A uniform blend of 60 wt % silica, 30 wt % alumina and 10 wt % titania was prepared as a reference material. Its titanium region spectrum (Fig. 5d) has a peak about half that of the titanium-rich area, shown in Fig. 5c. However, it is not possible to calculate a local $TiO_2$ concentration using EDXRA because matrix and orientation effects are not well defined for this type of rough sample. We estimate that these areas are at least 10% $TiO_2$ by weight, indicating that titania is not uniformly distributed throughout the catalyst particles. These titania inclusions originate as 1 to 5 $\mu$m particles in some kaolin clays and appear relatively unaffected by catalyst preparation or use in cracking units. The morphology of these particles cannot be distinguished from gel and their distribution must be determined by elemental X-ray mapping.

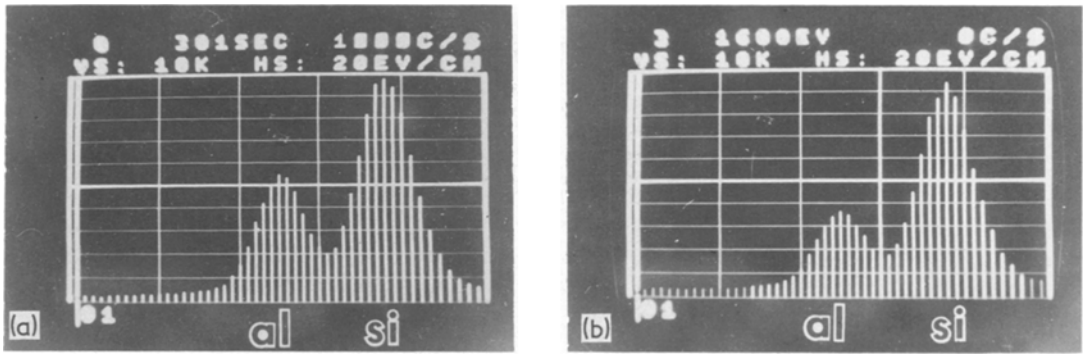


*Figure 4* Comparison of aluminium and silicon X-ray peaks of catalyst components. Clay Al peak – 5500 counts, zeolite Al peak – 3600 counts.

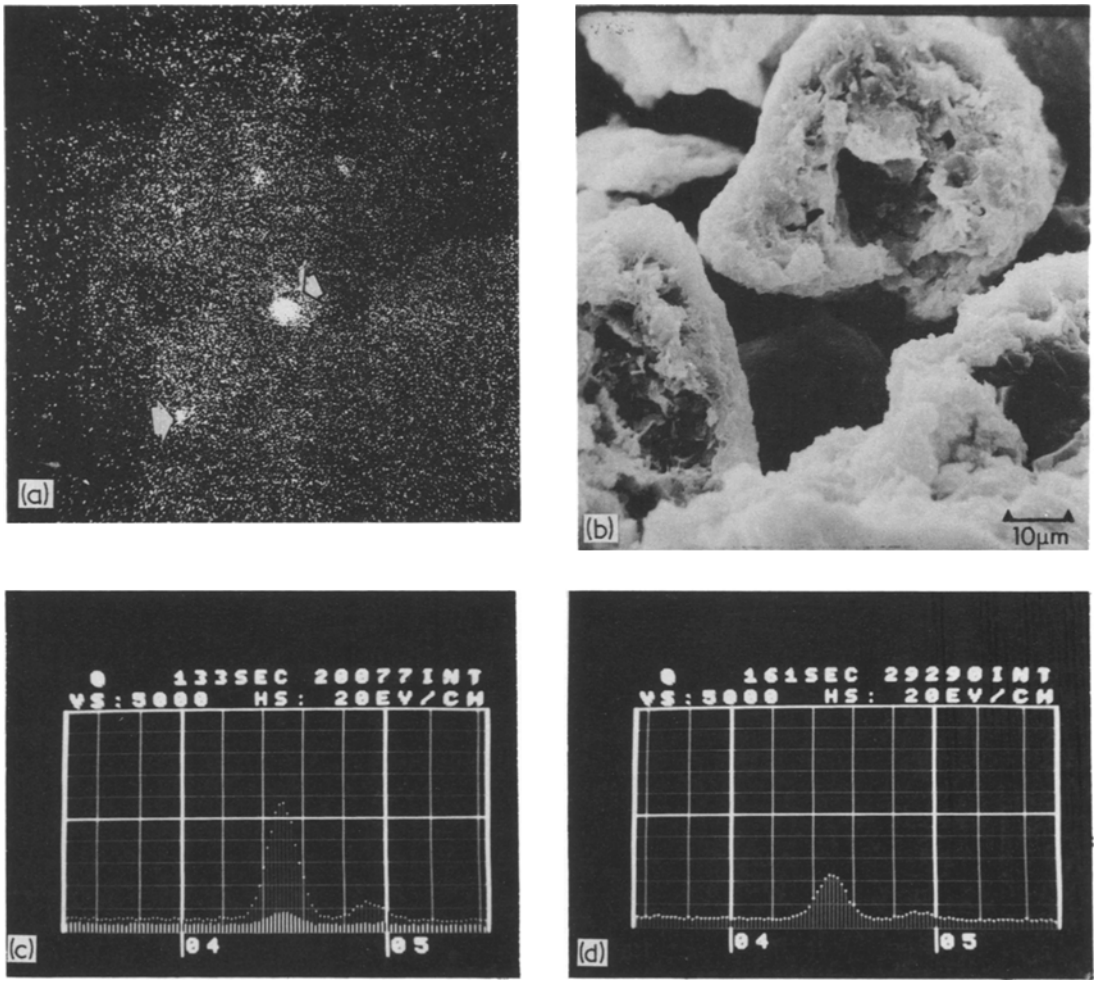


*Figure 5* (a) Titanium distribution in fractured catalyst particle, × 850. Arrows indicate several titanium inclusions. (b) Electron micrograph of same particle, × 850. (c) Titanium region X-ray spectra of inclusion compared with averaged field. Light lines represent inclusion, bright lines represent averaged field. (d) Titanium region X-ray spectrum of 60% $SiO_2$ –30% $Al_2O_3$ –10% $TiO_2$ reference material.

We are unable to detect sodium at the levels commonly found in cracking catalyst because of absorption of the sodium X-rays by the beryllium window of our X-ray analyser and by the gold–palladium coating. Iron may originate from the materials used to manufacture catalyst or from wear of steel equipment used during preparation or use in cracking units. Sulphur cannot be detected at the levels commonly found in cracking catalysts when gold–palladium alloy is used to coat the sample, because the gold *M* line overlaps the sulphur *K* line. In this situation silver is used as a coating. Other metals such as vanadium and nickel have been detected at concentrations of about 0.1 wt % but are often found in equilibrium catalysts at levels below the detection limits of an energy dispersive analyser. These metals originate in the crude oil from which the feed to the catalytic cracking unit is obtained.

In the future, the ability to detect low atomic number elements and lower levels of minor components may be improved by the use of fully focusing wave length dispersive spectrometers attached to the SEM column. However, analysis will take considerably longer since each element is detected individually and the low beam currents available in the SEM result in a relatively low count rate.

Scanning electron microscopy clearly reveals the shape and particle size distributions of the

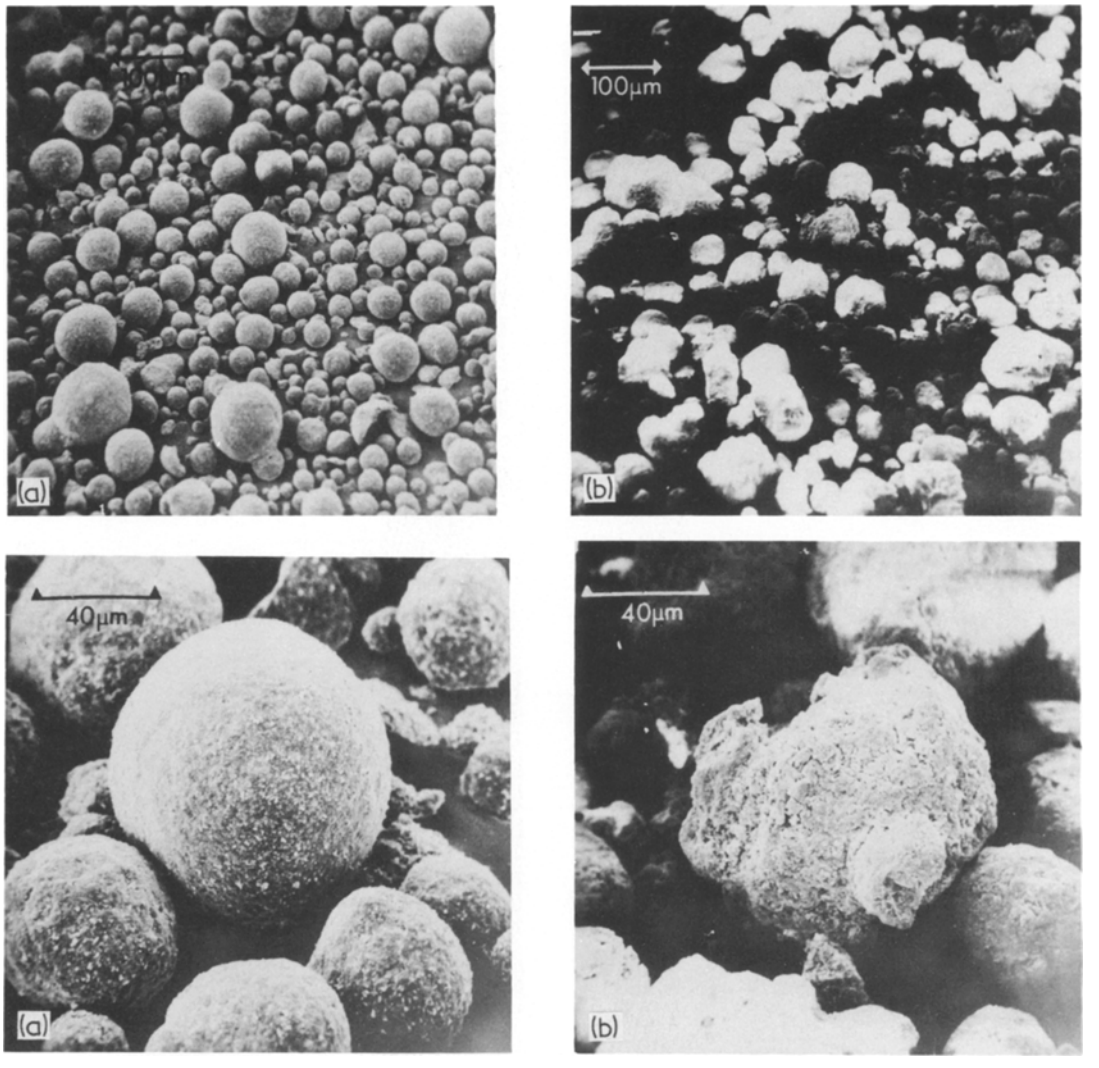


*Figure 6* (a) Cracking catalyst prepared from high solids slurry, × 85 and 425. (b) Cracking catalyst prepared from low solids slurry, × 85 and 425.

formed catalyst microspheres. However, the distribution observed in a micrograph does not coincide with micromesh analysis, usually used to determine size distribution. This technique is based on weight percentage within a given size range, rather than the number of particles within a certain range observed by SEM. The largest dimension of a particle determines which size screen in the set will trap it. Irregularities in particle shape can be observed in scanning electron micrographs. Fig. 6 compares two catalyst preparations of different particle shape that have approximately the same particle size distributions, indicated by the micromesh data of Table II. These catalysts were prepared from slurries of different chemical composition and solids content prior to final spray drying. The higher magnification micrographs show differences in surface texture. When material protrudes unevenly from the surface of a microsphere it is more likely to be worn away by colli-

TABLE II Micromesh particle size distribution

| Size range (μm) | Fresh catalyst (wt %) | | Used catalyst wt % |
|---|---|---|---|
| | A | B | C |
| 0–20 μm | 3 | 3 | 0 |
| 20–40 | 15 | 13 | 6 |
| 40–80 | 47 | 51 | 67 |
| 80–105 | 19 | 21 | 20 |
| 105–149 | 14 | 11 | 6 |

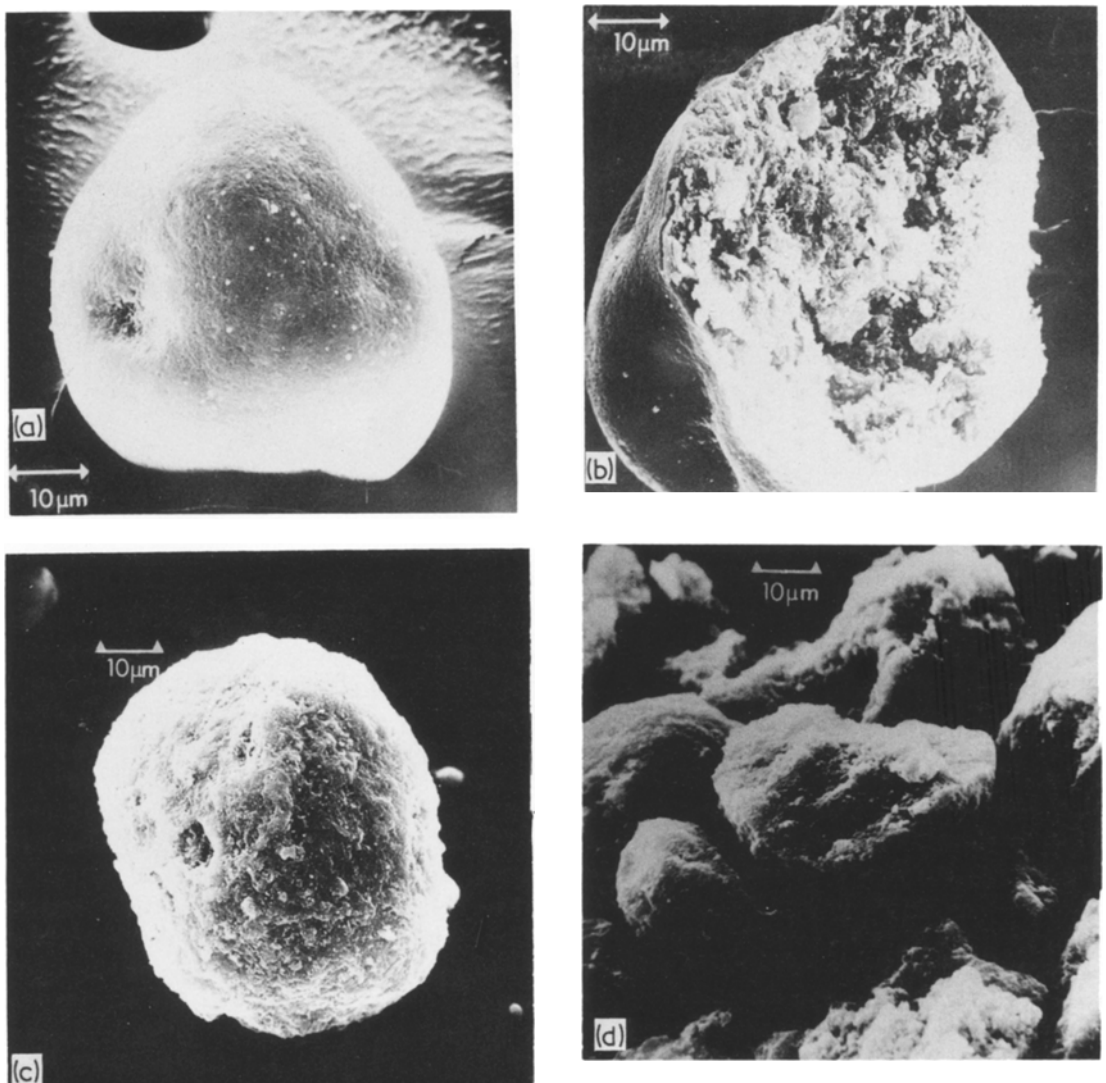


*Figure 7*(a) Surface of equilibrium cracking catalyst, X 850. (b) Interior of equilibrium cracking catalyst, X 850. (c). Surface of fresh cracking catalyst, X 850. (d) Interior of fresh cracking catalyst, X 850. (e) Low magnification field of used catalyst. Arrows point to surface depressions, X 85.

sions occurring during fluidization. Particles with a noticeable deviation from spherical shape offer more surface for collision and are thus more likely to attrite than perfect spheres. The more spherical, smooth particles of Fig. 6a are more attrition resistant when fluidized than those of Fig. 6b. In addition to the contribution of sphericity, molecular forces binding microsphere components together play a major role in determining resistance to attrition. Hence, deviation of particle shapes from perfect spheres cannot be the sole measure of catalyst hardness.

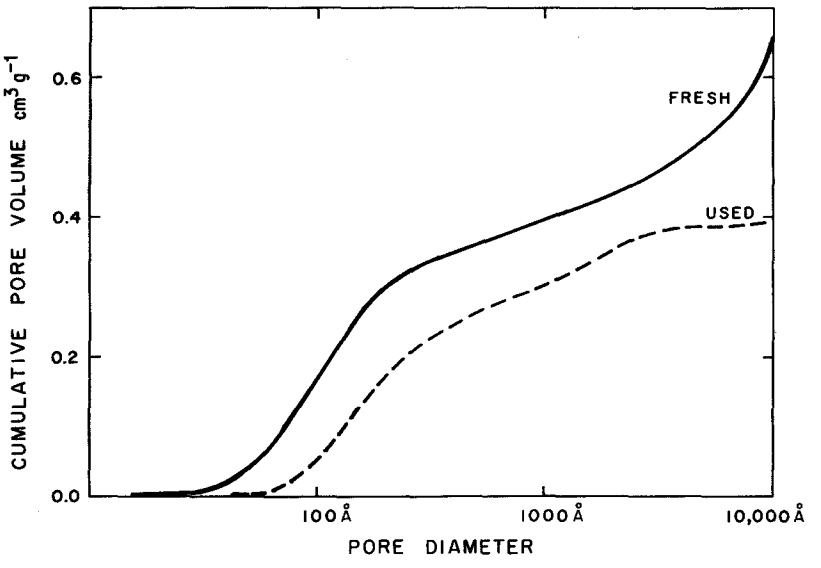


*Figure 8* Pore size distribution determined by mercury penetration of fresh and used catalyst.

## 3.2. Effects of process conditions on microstructure

Used catalyst removed from fluid cracking units has rounded, smooth surface texture (Fig. 7a) compared to fresh material (Fig. 7c). The irregularities appearing on the surface of fresh material are abraded when the catalyst is fluidized and circulated in the cracking process. Some surface sintering may occur and coke deposition may also account for the smoother appearance of used catalyst surface. However, in spite of the apparent loss of porosity on the surface of the microsphere, the activity of used catalysts averages about 70 vol. % conversion, similar to that obtained after steam deactivation of fresh catalyst. When we examine fractured, used catalyst microspheres (Fig. 7b) we observe that the interior of the catalyst remains porous and that the smooth surface is a thin shell, less than 0.2 $\mu$m thick. A plot of pore size distribution obtained by mercury penetration [16] shows loss of porosity at both the high and low end of the distribution (Fig. 8). Table III compares surface area and pore volume data for the used catalyst sample from which the particles in Figures 7a and b have been selected, with fresh catalyst of the same grade. Pores in the 100 to 4000 Å range are stable in the environment encountered in a refinery cracking unit. Fig. 7e is a low magnification micrograph of a field of used catalyst particles. In comparison with the low magnification fields of Fig. 6a and b, there are fewer particles smaller than 40 $\mu$m or larger than 105 $\mu$m. These results are consistent with the micromesh analysis listed in Table II.

The ability of a cracking catalyst to withstand destruction in a fluidized cracking unit is measured

TABLE III Pore size distributions of typical cracking catalyst

| Pore size range (Å) | Incremental pore volume ($cm^3 g^{-1}$) | | |
|---|---|---|---|
| | Fresh | Used | Steamed* |
| 14–100 | 0.17 ± 0.02† | 0.06 ± 0.01† | 0.06 ± 0.01† |
| 100–600 | 0.20 ± 0.02† | 0.21 ± 0.02† | 0.19 ± 0.02† |
| 600–4 000 | 0.12 ± 0.01‡ | 0.11 ± 0.01‡ | 0.11 ± 0.01‡ |
| 4 000–10 000 | 0.10 ± 0.01‡ | 0.01 ± 0.002‡ | 0.09 ± 0.01‡ |
| | Surface area ($m^2 g^{-1}$) | | |
| | 280 ± 20† | 95 ± 10† | 110 ± 10† |

*825° C, 20% steam, 12 h.
†Nitrogen adsorption.
‡Mercury penetration.

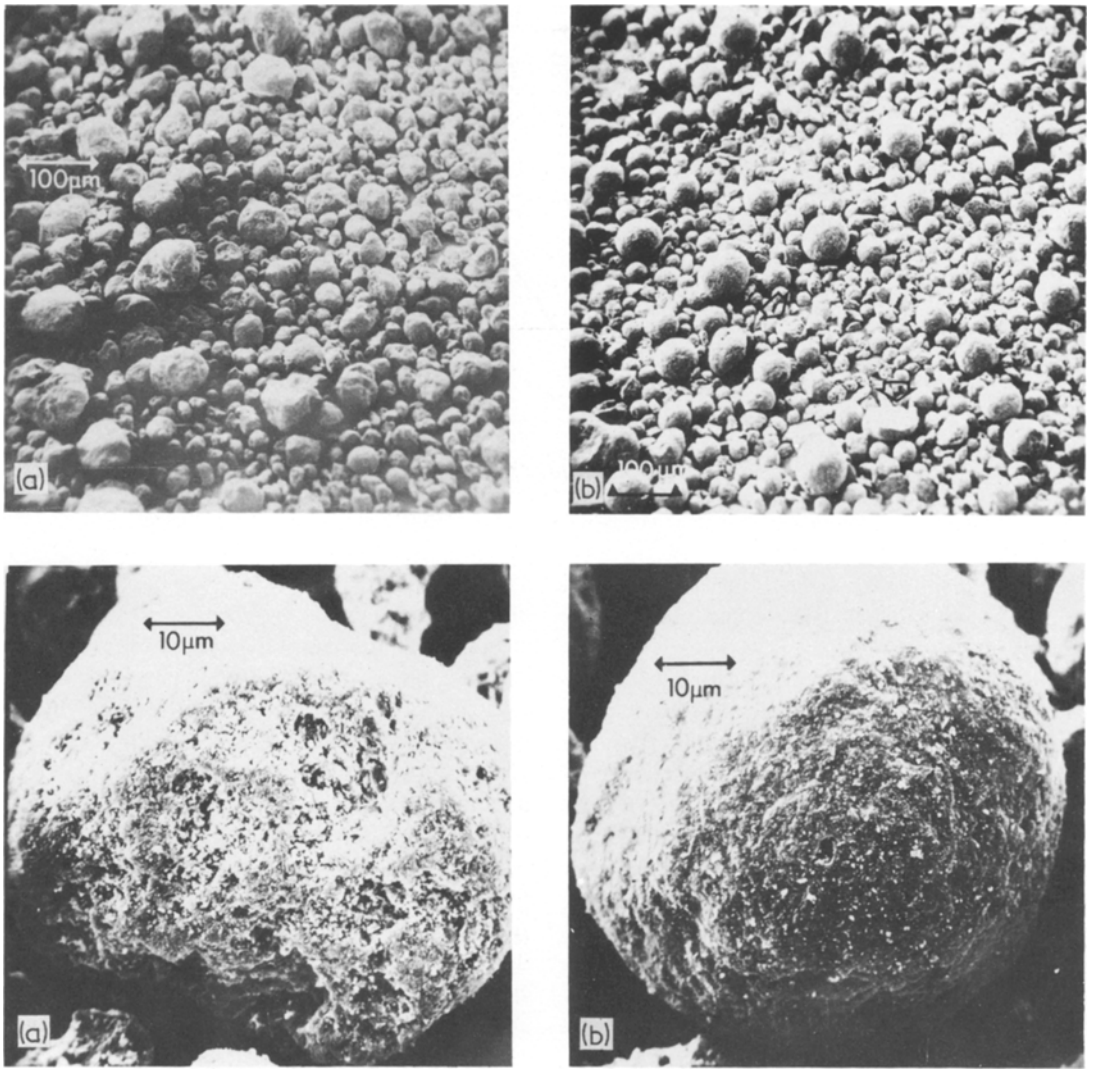


*Figure 9* (a) Surface of typical cracking catalyst after 3 h attrition, × 85 and 850. (b) Surface of resistant cracking catalyst after 3 h attrition, × 85 and 850.

by laboratory simulation of field attrition. It has been reported that the distribution of fine particles attrited from the surfaces of silica–alumina cracking catalysts could be best explained by wearing of particles from the surfaces of microspheres rather than fracture of the particle into intermediate sized fragments and subsequent breakdown into smaller particles [17]. Fig. 9a shows attrited catalyst where surface wear is clearly evident (relatively soft catalyst). The relatively soft catalyst sample lost 32% to fines during attrition testing, whereas the attrition resistant catalyst lost only 15%. Fig. 9b shows that the surface of the attrition resistant catalyst remained nearly intact. The low magnification micrograph shows many fractured, rather than worn, particles. Fracture of the microspheres may be caused by the more severe environment encountered by the particles in the laboratory test compared to use in fluid cracking units.

Cracking catalysts are subjected to thermal and steam treatments in the laboratory to simulate performance in cracking units [14]. Edgar [11] has shown that while volatile material amounting to about 10% of the original catalyst weight is removed by thermal shock at 760° C, the particle

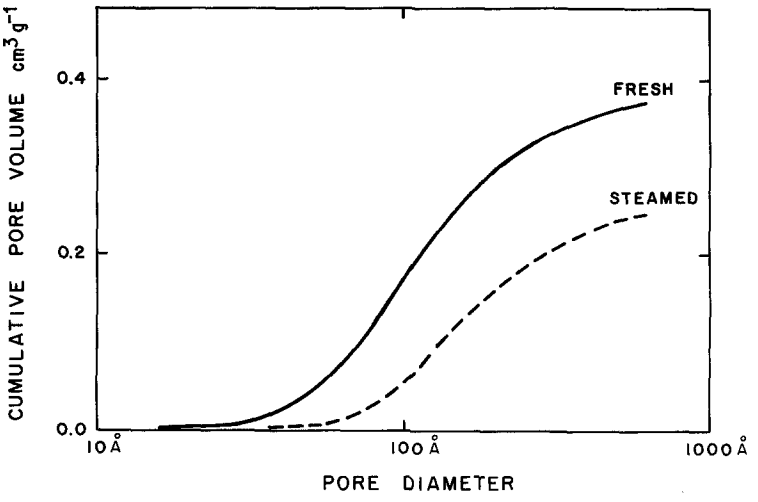


*Figure 10* Pore size distribution determined by nitrogen adsorption of fresh and steam deactivated catalyst.

integrity is maintained. Hence, fresh microspheres are not destroyed when injected into the cataytic cracking unit.

The purpose of a steam deactivation is to simulate the deactivation that fresh catalyst receives when added to a refinery cracking unit. There is a substantial decrease in surface area and a loss of porosity in the small pore size range. Fig. 10 and Table III compare a typical pore size distribution obtained by nitrogen absorption [18] for the same catalyst grade, fresh and after steam deactivation. Since the changes occur in pores whose openings are too small to be resolved by the scanning electron microscope, the morphology of steam deactivated catalyst closely resembles fresh material. Loss in catalytic activity occurs because of a decrease in acidic surface hydroxyls as the result of steaming. In the case of catalysts promoted with zeolites, this loss of acidity is related to loss of crystallinity in the zeolite component. Only in extreme cases where total collapse of all pore structure occurs can complete loss of activity be attributed to sintering of the catalyst. When a catalyst is deactivated in a more severe environment than the standard treatment, major morphological differences may be observed by SEM. Fig. 11a shows the surface of a catalyst normally deactivated at 730° C in a 100% steam atmosphere for 8 h after deactivation at 785° C at the same steam level and treatment time. This micrograph

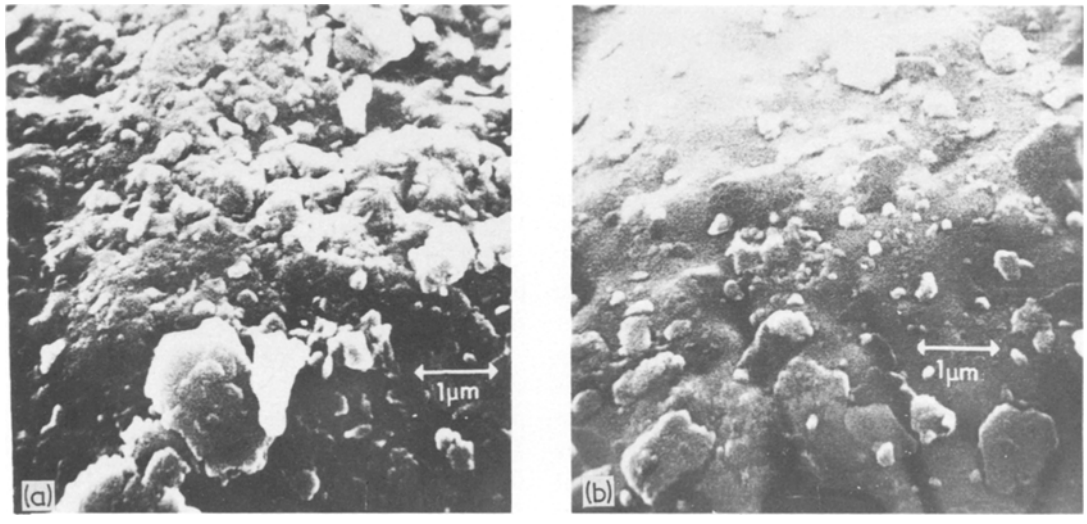


*Figure 11* (a) Catalyst surface after 760° C steaming, × 8500. (b) Catalyst surface after 850° C steaming, × 8500.

indicates that macroporosity is still retained. However, when the temperature is raised to 840° C, sintering is observed (Fig. 11b), the surface area drops below $10\,m^2\,g^{-1}$ and the catalyst is inactive.

## 4. Conclusions

The texture of surfaces of amorphous aluminosilicate cracking catalyst microspheres, which have relatively low activity for conversion of petroleum fractions to gasoline (petrol), cannot be readily distinguished from that of catalysts containing zeolites, which produce high conversion. However, the zeolite catalyst can be identified by examining scanning electron micrographs of fractured microspheres which show the zeolite, gel and clay components. Variations in particle size and morphologies of these components, which range in size from 0.1 to 5 $\mu$m, can only be observed by SEM in the formed microspheres. The spatial resolution and depth of field of an optical microscope are inadequate to see these components. Catalyst microspheres are too thick for direct transmission electron microscopy, while thin sections or replicas produce artefacts that produce a distorted representation of the distribution of components in a microsphere. In addition, SEM aids catalyst preparation by monitoring microsphere size and shape distribution.

The energy dispersive X-ray analyser assists in the identification of distinct morphological features of cracking catalysts and often reveals differences in chemical composition that would not be suspected from simple microscopic examination. For example, comparison of relative aluminium and silicon X-ray peaks confirms the morphological identifications of clay and zeolite in a formed catalyst microsphere interior. The single element mapping of titanium in clay-containing catalyst located concentrations of titania that did not have distinct morphology, at levels higher than the average content determined by conventional chemical analysis. The EDXRA is also used for qualitative comparison of the distribution of exchangable elements, used to enhance activity and stability, between promoter and matrix.

The morphology of fluidizable cracking catalyst changes after use in refinery cracking units. Low magnification micrographs show a particle size distribution, consistent with micromesh analysis, which indicates removal of less than 40 $\mu$m particles from the circulating inventory of catalyst and reduction of large particles to less than 100 $\mu$m equivalent sphere diameter by attrition. The surfaces of individual particles appear sintered, yet the used catalyst is still active. Examination of fractured particles shows that the interior is still porous and that the compacted surface is only a thin shell. Pore size distribution data indicate that pores in the range from 100 to 4000 Å are only slightly altered when cracking catalysts are used in refineries.

Substantial surface wear, producing "craters", is observed after relatively soft catalysts are subjected to a laboratory attrition test, while resistant grades remain relatively intact under the same conditions. Scanning electron micrographs of used catalyst show that softer catalyst grades have some particles with depressions (Fig. 7e) which may be rounded craters. Harder grades appear to have smoother surfaces.

When catalysts are steam deactivated, under standard conditions, very little change is observed in the morphology of the microsphere. Only catalysts deactivated in a very severe steam environment exhibit significant morphological modifications.

Our investigations indicate that the activity of cracking catalysts cannot be directly correlated with their morphology observed in scanning electron micrographs. Nevertheless, the SEM combined with the EDXRA accessory allows us to observe microscopic features, not detected by analytical methods that average properties over thousands of particles, which are significant in the preparation and use of fluidizable cracking catalysts.

## Acknowledgements

We wish to thank the Davison Chemical Division of W. R. Grace & Co for permission to publish this paper. The micrographs were taken by Mr Floyd Sykes. Porosimetry measurements were made by Mr James Foard and Mr Paul Sponaugle.

## References

1. C. R. ADAMS and H. H. VOGE, *J. Phys. Chem.* **61** (1957) 722.
2. J. D. LAWSON and H. F. ROSE, *Ind. Eng. Chem. Prod. Res. Dev.* **9** (1970) 317.
3. D. W. PARIS, I. G. ROCHOW, F. G. ROWE, M. L. FULLER, P. F. KERR and P. K. HAMILTON, "Electron Micrographs of Reference Clay Minerals", American Petroleum Institute Preliminary Report No. 6 (Columbia University Press, New York, 1950).
4. O. C. WELLS, "Scanning Electron Microscopy" (McGraw Hill, New York, 1974).

5. S. D. ROBERTSON, J. FREEL and R. B. ANDERSON, *J. Catal.* **24** (1972) 130.
6. J. B. MOFFAT and J. F. BRAUNEISEN, *ibid* **30** (1973) 66.
7. D. FAULKNER, N. H. SAGERT, E. E. SEXTON and R. C. STYLES, *ibid* **25** (1972) 446.
8. B. WALDIE, *J. Mater. Sci.* **4** (1969) 648.
9. A. BOSSI, G. LEOFANTI, E. MORETTI and N. GIORDANO, *ibid* **8** (1973) 1101.
10. A. M. REIMSCHUSSEL and R. J. FREDERICKS, *ibid* **4** (1969) 885.
11. M. D. EDGAR, *Oil Gas J.* (1973) 110.
12. J. S. MAGEE and W. S. BRIGGS, U.S. Patent 3 650 988 (1972).
13. R. W. BAKER, F. G. CIAPETTA, C. P. WILSON, JUN and P. K. MAHER, U.S. Patent 3 425 956 (1969).
14. J. S. MAGEE and J. J. BLAZEK, Advances in Chemistry, "Zeolite Chemistry and Catalysis", edited by J. A. Rabo (American Chemical Society, Washington, D.C., 1976).
15. L. S. BIRKS, "Electron Probe Microanalysis", Chemical Analysis, Vol. 17 (Wiley Interscience, New York, 1971).
16. L. C. DRAKE, *Ind. Eng. Chem.* **41** (1949) 780.
17. J. E. GWYN, *AIChE J.* **15** (1969) 35.
18. E. P. BARRETT, L. G JOYNER and P. P. HALENDA, *J. Amer. Chem. Soc.* **73** (1951) 373.

Received 3 March and accepted 21 June 1976.